Identification of grain boundary contours at atomic scale

Benjamin Berkels[1], Andreas Rätz[2], Martin Rumpf[1], and Axel Voigt[2]

[1] Institut für Numerische Simulation,
Rheinische Friedrich-Wilhelms-Universität Bonn,
Nussallee 15, 53115 Bonn, Germany
{benjamin.berkels, matrin.rumpf}@ins.uni-bonn.de,
WWW home page: http://numod.ins.uni-bonn.de/
[2] Crystal Growth Group, Research Center caesar
Ludwig-Erhard-Allee 2, 53175 Bonn, Germany

Abstract. Nowadays image acquisition in materials science allows the resolution of grains at atomic scale. Grains are material regions with different lattice orientation which are typically not in equilibrium. At the same time, new microscopic simulation tools allow to study the dynamics of such grain structures. Single atoms are resolved in the experimental and in the simulation results. A qualitative study of experimental images and simulation results and the comparison of simulation and experiment requires the robust and reliable extraction of mesoscopic properties from these microscopic data sets. Based on a Mumford–Shah type functional, grain boundaries are described as free discontinuity sets at which the orientation parameter for the lattice jumps. The lattice structure itself is encoded in a suitable integrand depending on the local lattice orientation. In addition the approach incorporates solid–liquid interfaces. The resulting Mumford–Shah functional is approximated with a level set active contour model following the approach by Chan and Vese. The implementation is based on a finite element discretization in space and a step size controlled gradient descent algorithm.

AMS Subject Classifications (2000): 65M60, 68U10, 74E15

1 Introduction

The goal of this paper is to present a method for joint segmentation and orientation classification in materials science. For many problems in materials science on an atomic microscale, it is essential to link the underlying atomic structure to the material properties (electrical, optical, mechanical, etc.). The actual material properties are usually determined on a mesoscopic length scale on which non–equilibrium structures exist, which form and evolve during material processing. For example, the yield strength of a polycrystal varies with the inverse square of the average grain size. Grains are material regions with different lattice orientation which are typically not in equilibrium. Experimental tools such as TEM

(transmission electron microscopy) [12] today allow measurements down to an atomic resolution (cf. Fig.1). A reliable extraction of grains and grain boundaries
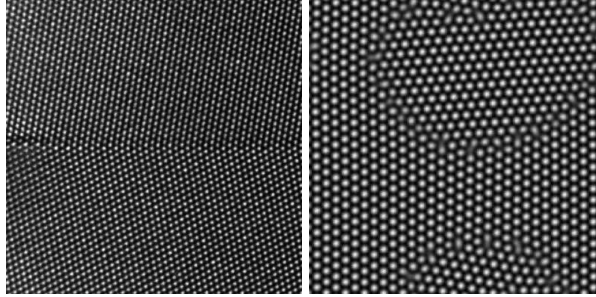

Fig. 1. On a TEM image (left), light dots render atoms from a single atom layer of aluminum, in particular this image shows a $\Sigma 11(113)/[\bar{1}00]$ grain boundary [12] (courtesy of Geoffrey H. Campbell, Lawrence Livermore National Laboratory). Nowadays, there are physical models like the phase field crystal model which enable the numerical simulations of grains. Indeed, a time step from a numerical simulation (right) on the microscale shows an similar atomic layer. In both images, grain boundaries are characterized by jumps in the lattice orientation.

from these TEM-images is essential for an efficient material characterization. On the other hand, recent numerical simulation tools have been developed for physical models of grain formation and grain dynamics on the atomistic scale. Concerning such simulations, we refer to numerical results obtained from a phase field crystal (PFC) model [10] derived from the density function theory (DFT) of freezing [23]. Its methodology describes the evolution of the atomic density of a system according to dissipative dynamics driven by free energy minimization. The resulting highly nonlinear partial differential equation of sixth order is solved applying a finite element discretization [20]. These simulations in particular will allow a validation of the physical models based on the comparison of mesoscopic properties such as the propagation speed of grain boundaries. The formation of grains from an undercooled melt happens on a much faster time scale than their subsequent growing and coalescence. The evolution of grain boundaries at later stages of the process is of particular interest. Fig. 1 and 2 show a comparison of experimental (TEM) and numerically simulated (PFC) single grain boundaries on the atomic scale and the nucleation of grains, respectively. In this paper, we aim at a reliable extraction of grain boundaries and in addition of interfaces between the liquid and the solid phase. Thus, we apply a variational approach based on the description of the interfaces by level sets. Our focus is on the post processing of phase field simulation results, but we will as well demonstrate the applicability of our approach to experimental images.

Image classification has extensively been studied in the last decades. It consists of assigning a label to each point in the image domain and is one of the basic problems in image processing. Classification can be based on geometric
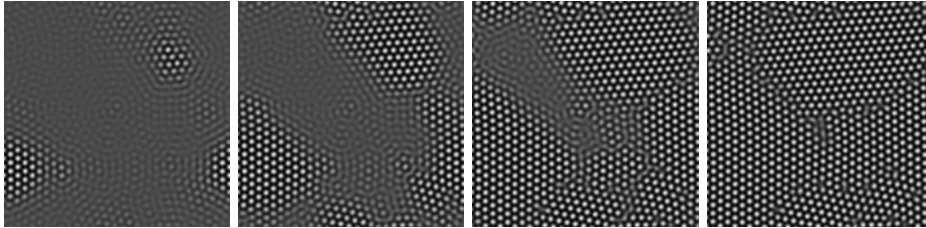
Fig. 2. Nucleation of grains in a phase field crystal simulation.

and on texture information. Many models have been developed either based on region growing [24, 19, 6], on statistical approaches [4, 5, 14, 15], and in particular recently on variational approaches [3, 1, 8, 16, 26].

The boundaries of the classified regions can be considered as free discontinuity sets of classification parameters, which connects the problem with the Mumford–Shah approach [17] to image segmentation and denoising. A robust and efficient approximation of the Mumford–Shah functional has been presented by Chan and Vese [7] for piecewise constant image segmentation and extended to multiple objects segmentation based on a multiphase approach [25]. Thereby, the decomposition of the image domain is implicitly described by a single or multiple level set functions (for a review on level sets we refer to [18, 22]). In [21], their approach has been further generalized for the texture segmentation using a directional sensitive frequency analysis based on Gabor filtering. Texture classification based on the energy represented by selected wavelet coefficients is investigated in [2]. Inspired by the work of Meyer [16] on cartoon and texture decomposition, the classification of geometrical and texture information has been investigated further in [3]. There a logic classification framework from [21] has been considered to combine texture classification and geometry segmentation. A combination of level set segmentation and filter response statistics has been considered for texture segmentation in [11]. For a variational texture segmentation approach in image sequences based on level sets we refer to [9].

Our method to be presented here differs to the best of our knowledge significantly from other variational approaches in the literature. Our focus is not on a general purpose texture classification and segmentation tool but on the specific application in materials science. Texture segmentation can be regarded as a two–scale problem, where the microscale is represented by the structure of the texture and the macroscale by the geometric structure of interfaces between differently textured regions. In this sense, we have strong a priori knowledge on the geometric structure of the texture on the microscale and incorporate this directly into the variational approach on the macroscale. Thus, the scale separation is more direct than in other approaches based on a local, direction sensitive frequency analysis.

2   A Mumford–Shah model for the lattice orientation

We consider a single atom layer resolved on the microscale. In the phase field simulation results as well as in the experimental images, single atoms are represented by blurry, dot-like structures. These dots are either described via the image intensity of the TEM image or the phase field function from the simulation. Let us denote this intensity or phase field by a function $u : \Omega \subset \mathbb{R}^2 \to \mathbb{R}$, where Ω is the image domain or the computational domain, respectively. Furthermore, we introduce the lattice orientation as a function $\alpha : \Omega \subset \mathbb{R}^2 \to \mathbb{R}$. In addition we consider the decomposition of the domain Ω into a solid phase Ω_S and a liquid phase Ω_L. The solid domain Ω_S is further partitioned into grains, each of them characterized by a constant lattice orientation α. The grain boundaries form the jump set of the orientation function α. In the following section, we will first introduce a Mumford–Shah type model for the segmentation of grains and then expand this model to incorporate as well liquid–solid interfaces.

2.1   Segmenting grain boundaries

As already discussed in the introduction, grains are characterized by a homogeneous lattice orientation. At first, let us suppose that there is no liquid phase. Thus, the whole domain Ω is partitioned into grain subdomains. The lattice is uniquely identified by a description of the local neighborhood of a single atom in the lattice. In a reference frame with an atom at the origin, the neighboring atoms are supposed to be placed at positions q_i for $i = 1, \cdots, m$, where m is the number of direct neighbors in the lattice. In case of a hexagonal packing each atom has six direct neighbors at equal distances and we obtain

$$q_i := d \left(\cos \left(i \frac{\pi}{3} \right), \sin \left(i \frac{\pi}{3} \right) \right) \quad i = 1, \cdots, 6 \,.$$

Here $d > 0$ denotes the distance between two atoms. If the lattice from the reference configuration is now rotated by an angle α and translated to a position x, the neighboring atoms are located at the positions $x + M(\alpha)q_i$ where $M(\alpha)$ is the matrix representation of a rotation by α, i.e.

$$M(\alpha) := \begin{pmatrix} \cos \alpha & -\sin \alpha \\ \sin \alpha & \cos \alpha \end{pmatrix}.$$

Let us suppose that θ is a suitable threshold for the identification of the atom dots described via the function u and define the indicator function

$$\chi_{[u>\theta]}(x) := \begin{cases} 1; & u(x) > \theta \\ 0; & \text{else} \end{cases} \,.$$

Then, for a given lattice orientation α and a point x with $\chi_{[u>\theta]}(x) = 1$, we expect $\chi_{[u>\theta]}(x + M(\alpha)q_i) = 1$ as well for $i = 1, \cdots, m$. Let us suppose that the average radius of a single atom dot is given by r and define the maximal lattice spacing $d := \max_{i=1\cdots,m} |q_i|$. Next, we consider an indicator function $f :$

$\Omega \times \mathbb{R} \to \mathbb{R}$ depending on the position x and on a lattice orientation α and given by

$$f(x, \alpha) = \frac{d^2}{r^2} \chi_{[u>\theta]}(x) \Lambda \left(\left(\chi_{[u>\theta]}(x + M(\alpha)q_i) \right)_{i=1,\cdots,m} \right). \qquad (1)$$

Here, $(\chi_i)_{i=1,\cdots,m}$ with $\chi_i := \chi_{[u>\theta]}(x + M(\alpha)q_i)$ is the vector of translated and rotated characteristic functions and $\Lambda : \{0,1\}^m \to \mathbb{R}$ a function attaining its global minimum at $(1, \cdots, 1)$ and $\Lambda(1, \cdots, 1) = 0$. The scaling $\frac{d^2}{r^2}$ ensures a uniform upper bound of order 1 (in particular independent of d and r) for the integral of f over Ω. One easily verifies that $f(x, \alpha) = 0$ if x is inside a grain with orientation α and its distance to the grain boundary is at least d. Possible choices for Λ are for instance

$$\Lambda(\chi_1, \cdots, \chi_m) := \frac{1}{m} \sum_{i=1,\cdots,m} (1 - \chi_i), \quad \text{or} \qquad (2)$$

$$\Lambda(\chi_1, \cdots, \chi_m) := 1 - \prod_{i=1,\cdots,m} \chi_i. \qquad (3)$$

In the numerical experiments we found (3) to be the most suitable choice.

For a fixed number of n grains Ω_j with lattice orientation α_j for $j = 1, \cdots, n$, we consider a piecewise constant function

$$\alpha = \sum_{j=1,\cdots,m} \alpha_j \chi_{\Omega_j}$$

reflecting the orientation within the grains. Here, the grain domains Ω_j and the grain orientations α_j form the set of unknowns. Now, we define a functional E_{grain} acting on the set of lattice orientations α_j and open grain domains Ω_j in the spirit of the Mumford–Shah functional:

$$E_{\text{grain}}[(\alpha_j, \Omega_j)_{j=1,\cdots,m}] := \sum_{j=1,\cdots,m} \left(\int_{\Omega_j} f(x, \alpha_j) \, dx + \eta \text{Per}(\Omega_j) \right),$$

where $\{\Omega_j\}_j$ is a partition of the domain Ω, i.e. $\Omega_j \cap \Omega_i \neq \emptyset$ and $\bigcup_j \bar{\Omega}_j = \Omega$. $\text{Per}(\Sigma)$ denotes the perimeter of a set Σ, i.e. the length of the boundary of the set. A minimizer of this energy is considered as a reliable identification of lattice orientations and corresponding grains. In case of only two different lattice orientations α_1 and α_2 and corresponding (possibly not connected) domains Ω_1 and Ω_2, we can formulate the variational problem as a problem on the binary function α and the interface Γ_G between the two sets Ω_1 and Ω_2 and obtain (up to the constant term $\text{Per}(\Omega)$) the energy

$$E_G[\alpha_1, \alpha_2, \Gamma_G] := \int_{\Omega_1} f(x, \alpha_1) \, dx + \int_{\Omega_2} f(x, \alpha_2) \, dx + 2\eta \mathcal{H}^1(\Gamma_G)$$

where $\mathcal{H}^1(\cdot)$ denotes the one-dimensional Hausdorff measure.

2.2 Simultaneously detecting a liquid–solid interface

Let us now incorporate the distinction between solid and liquid phase into our variational model. In particular in the simulation results, the solid state is characterized by prominent atom dots with large values of u. Indeed, taking into account threshold values θ_1 and θ_2, we suppose that $u(x) > \theta_2$ indicates an atom dot at position x and vice versa inter–atom regions are characterized by low values of u, i.e. $u(x) < \theta_1$. In the liquid regime there are neither very high nor low values of u, i.e. $u(x) \in [\theta_1, \theta_2]$. Unfortunately, the converse is not true. In transition regions between atom and hole in a solid region u will attain values between θ_1 and θ_2. But in these transition regions, the gradient of u exceeds a certain threshold $\epsilon > 0$. Thus, we assume x to be in the liquid phase Ω_L if $u \in [\theta_1, \theta_2]$ and $|\nabla u| \le \epsilon$. A variational description of the domain splitting into a liquid phase Ω_L and a solid phase is encoded in the energy

$$E_{\text{phase}}[\Omega_L] = \int_{\Omega_L} q(x)\,\mathrm{d}x + \int_{\Omega \setminus \Omega_L} 1 - q(x)\,\mathrm{d}x + \nu \mathrm{Per}(\Omega_L),$$

based on the indicator function

$$q(x) := 1 - \chi_{[u>\theta_1]}(x)\chi_{[u<\theta_2]}(x)\chi_{[|\nabla u|<\epsilon]}(x)$$
$$= \begin{cases} 0 & ;\text{ for } \quad u \in [\theta_1, \theta_2] \wedge |\nabla u| < \epsilon \\ 1 & ;\text{ else}. \end{cases}$$

Since $q = 1$ in the solid region the first term favors to remove solid phase points from Ω_L. On the other hand $q = 0$, in the liquid region. Hence, it is preferable to remove liquid parts from $\Omega \setminus \Omega_L$. In the usual spirit of the Mumford–Shah approach, the third term regularizes the boundary of Ω_L.

Now, we merge the two approaches above and simultaneously want to detect the liquid phase Ω_L and the solid phase $\Omega \setminus \Omega_L$ which itself is decomposed into grains Ω_j, such that $\bigcup_j \Omega_j = \Omega \setminus \Omega_L$. We end up with the following energy

$$E[\Omega_L, (\alpha_j, \Omega_j)_{j=1,\cdots,m}] := \mu \int_{\Omega_L} q(x)\,\mathrm{d}x + \mu \int_{\Omega \setminus \Omega_L} (1 - q(x))\,\mathrm{d}x + \nu \mathrm{Per}(\Omega_L)$$
$$+ \sum_{j=1,\cdots,m} \left(\int_{\Omega_j} f(x, \alpha_j)\,\mathrm{d}x + \eta \mathrm{Per}(\Omega_j) \right). \tag{4}$$

The primal decomposition is the one into a liquid and a solid domain. To reflect this in the variational formulation above we consider a relatively large constant μ. Indeed, we choose $\mu = 10$ and $\nu = \eta = 0.05$. Furthermore, in the application considered here we take into account the following values for the other constants involved: $\theta = 0.5$, $\theta_1 = 0.3$, $\theta_2 = 0.5$, $\epsilon = 1$ (artificial test data) or $\epsilon = 20$ (PFC simulation data).

In case of only two grain orientations α_1 and α_2 we can rewrite the energy and obtain

$$E[\Gamma_{LS}, \alpha_1, \alpha_2, \Gamma_G] := \mu \int_{\Omega_L} q(x)\,\mathrm{d}x + \mu \int_{\Omega \setminus \Omega_L} 1 - q(x)\,\mathrm{d}x \tag{5}$$

$$+ 2\nu \mathcal{H}^1(\Gamma_{LS}) + 2\eta \mathcal{H}^1(\Gamma_G)$$

$$+ \int_{\Omega_1} f(x, \alpha_1)\,\mathrm{d}x + \int_{\Omega_2} f(x, \alpha_2)\,\mathrm{d}x\,, \tag{6}$$

which now depends on a single grain interface Γ_G and the liquid–solid interface Γ_{LS}.

3 Chan–Vese type level set approach

To solve the above free discontinuity problems, we consider a Chan–Vese type approach and rewrite the variational formulation based on an implicit description of the domains via level set functions. We focus here on two different unknown grain orientations α_1 and α_2 and consider two level set functions ϕ and ψ. Here, ϕ is supposed to define the decomposition into a liquid and a solid domain, i. e. $\Omega_L = [\phi \geq 0]$ and $\Omega_S = [\phi < 0]$. Furthermore, to simplify the algorithm, we suppose the second level set function ψ to be defined on the whole domain Ω even though the grains described by this function are given as subsets of the solid domain. Indeed, we assume

$$\Omega_1 = [\phi < 0] \cap [\psi < 0]\,, \quad \Omega_2 = [\phi < 0] \cap [\psi > 0]\,.$$

Then, we end up with the following Chan–Vese type energy

$$E_{CV}[\phi, \alpha_1, \alpha_2, \psi] := \int_\Omega \mu(H(\phi)\,q(x) + (1 - H(\phi))\,(1 - q(x))) + 2\nu|\nabla H(\phi)|$$

$$+ (1 - H(\phi))\,(1 - H(\psi))\,f(x, \alpha_1)$$

$$+ (1 - H(\phi))\,H(\psi)\,f(x, \alpha_2)$$

$$+ 2\eta(1 - \beta H(\phi))|\nabla H(\psi)|\,\mathrm{d}x\,, \tag{7}$$

depending on the two level set functions ϕ, ψ and the two grain orientations α_1 and α_2. Here $H(\cdot)$ denotes the Heaviside function with $H(s) = 1$ for $s > 0$ and $H(s) = 0$ else. In case $\beta = 1$, the interface $[\psi = 0] \cap [\phi \geq 0]$ is not at all controlled by the energy. For $0 \leq \beta < 1$ we observe a difference between the original energy and the new level set formulation in terms of the length of the extension of the grain interface $[\psi = 0]$ in the liquid domain Ω_L, i.e. up to the constant length of the domain boundary $\partial \Omega$, $E_{CV} - E = 2\eta\beta\|H(\phi)\nabla H(\psi)\|_{var} = 2\eta\beta\mathcal{H}^1([\psi = 0] \cap [\phi \geq 0])$. Thus, the method will extend physical meaningful grain interfaces by shortest paths from the triple point on the liquid–solid interface to the boundary on the domain Ω. In the applications considered, we observed no artifacts from this algorithmic simplification.

The variational modeling of more than two grain orientations can be based on the multiple domain segmentation method by Chan and Vese [25] in a straight-forward way. In our current implementation, we confine to the case of only two orientations. The generalization is under development. As of now, we also only use $\beta = 0$.

4 Regularization and numerical minimization

Since H is not continuous we replace it by a smeared out Heavyside function. Here we again follow [7] and consider $H_\delta(x) := \frac{1}{2} + \frac{1}{\pi} \arctan\left(\frac{x}{\delta}\right)$ where $\delta > 0$. Let us emphasize that a desired guidance of the initial zero contours to the actual interfaces to be detected requires a non-local support of the regularized Heavy-side function. To numerically solve the problem, we apply a gradient descent in the two level set functions ϕ and ψ and the two orientation values α_1 and α_2. Different from the grey value segmentation via the original approach by Chan and Vese, the energy is not quadratic in these two unknowns and thus minimization over these two angles is already a non-linear problem. Hence, we have to compute the variation of the energy with respect to the level set functions ϕ, ψ and the orientations α_1 and α_2. For the variation of the energy with respect to the level set function ϕ we obtain

$$
\begin{aligned}
\langle \delta_\phi E_{CV}, \theta \rangle =& \mu \int_\Omega H'_\delta(\phi)(2q(x) - 1)\theta \, \mathrm{d}x - 2\nu \int_\Omega H'_\delta(\phi)\theta \, \nabla \cdot \left(\frac{\nabla \phi}{|\nabla \phi|} \right) \mathrm{d}x \\
& - \int_\Omega H'_\delta(\phi)\big((1 - H_\delta(\psi))f(x, \alpha_1) + H_\delta(\psi)f(x, \alpha_2)\big)\theta \, \mathrm{d}x \\
& - 2\eta\beta \int_\Omega H'_\delta(\phi) \, |\nabla H(\psi)| \, \theta \, \mathrm{d}x
\end{aligned}
$$

which reflects the sensitivity with respect to modifications of the implicit description of the liquid–solid interface. Grain boundary sensitivity is encoded implicitly in the variation with respect to the level set function ψ and we achieve

$$
\begin{aligned}
\langle \delta_\psi E_{CV}, \zeta \rangle =& \int_\Omega (1 - H_\delta(\phi))H'_\delta(\psi)(f(x, \alpha_2) - f(x, \alpha_1))\zeta \, \mathrm{d}x \\
& - 2\eta \int_\Omega H'_\delta(\psi)(1 - \beta H(\phi))\zeta \, \nabla \cdot \left(\frac{\nabla \psi}{|\nabla \psi|} \right) \mathrm{d}x \,.
\end{aligned}
$$

Finally, a variation of the energy with respect to one of the grain orientations – we exemplarily consider here α_1 – leads to

$$
\partial_{\alpha_1} E_{CV} = \int_\Omega (1 - H_\delta(\phi))(1 - H_\delta(\psi))\partial_\alpha f(x, \alpha_1) \, \mathrm{d}x \,.
$$

Armijo's rule [13] is considered as a step size control in the descent algorithm. We consider bilinear finite elements on the regular grid for the spatial discretization of the two level set functions ϕ and ψ. Each pixel of an experimental image

or each node of the regular simulation grid corresponds to a node of the finite element mesh.

The initialization of ϕ and ψ has a significant impact on the results of the numerical descent method. If initialized improperly, the minimization might get stuck in local minima far away from a desired global minimum. In particular, if ψ is initially set in such a way that the grain boundary interface is contained completely in the liquid phase, one frequently observes that ψ does not move in the gradient descent at all.

5 Numerical results

At first, we tested the algorithm on artificial test data, generated from homogeneous dots on a lattice with precisely the same lattice spacing as encoded in our algorithm. A simple blending between two such lattices with different orientation or with a constant grey image is used to artificially generate grain boundary type or liquid–solid type interfaces. Fig. 3 shows the identification of grain boundaries of different amplitude, whereas Fig. 4 demonstrates the extraction of a liquid–solid interface. Furthermore, in Fig. 4 a liquid–solid interface and a grain boundary have simultaneously been identified. Furthermore, we applied
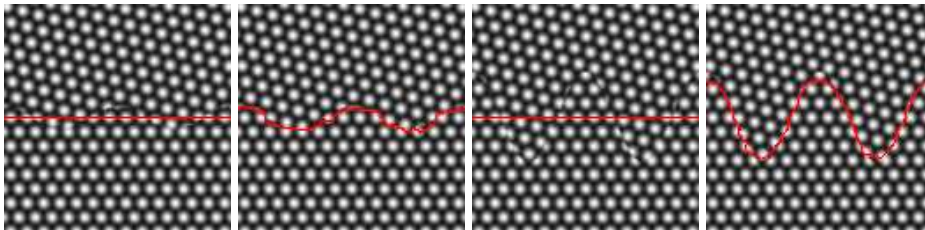

Fig. 3. Grain boundary detection on artificial test data: input images u (first and third picture) with initial zero level set of ψ and computed grain boundaries (second and fourth picture). Interfaces with different amplitude are considered in the first and second image pair.

our method to transmission electron microscopy images. These results, shown in Fig. 5, in particular demonstrate the robustness of the approach with respect to noise in the experimental data and natural fluctuations in the shape of the atom dots and the lattice spacing. In particular, let us emphasize that the variational method is capable to detect effects on an intermediate scale like the oscillating pattern of the interface in the second picture pair. Finally, we considered the identification of grain boundaries and liquid–solid interfaces in simulation data from a phase field crystal model. Fig. 6 shows the extraction of a grain boundary and the computation of both types of interfaces.
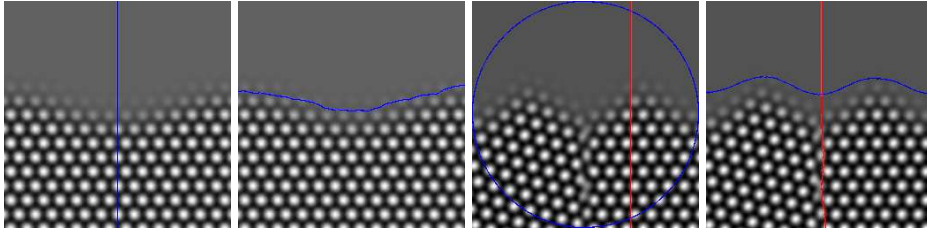
Fig. 4. Liquid–solid interface detection on artificial test data: input image u (first picture) with initial zero level set of ϕ and computed interface (second picture). Combined grain boundary and liquid–solid interface detection on artificial test data: input image u (third picture) with the initial grain boundary in red and the initial liquid–solid interface in blue, final grain boundary and liquid–solid interface location (fourth picture).
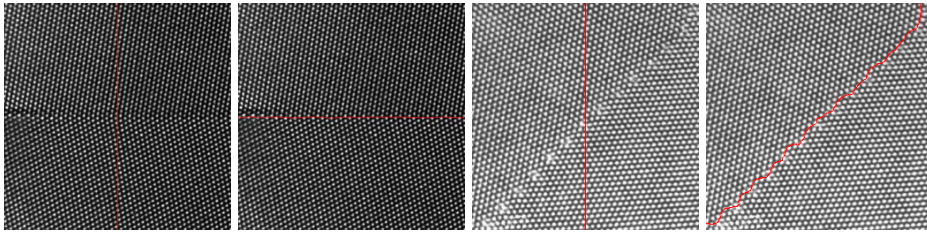

Fig. 5. Two results of grain boundary detection on TEM-images: input images u (first and third picture) with initial position of the zero level set of ψ, finally detected grain boundaries (second and fourth picture). The TEM-image in the first picture pair is courtesy of Geoffrey H. Campbell, Lawrence Livermore National Laboratory (compare Fig. 1), the image used in the second picture pair is courtesy of David M. Tricker (Department of Materials Science and Metallurgy, University of Cambridge) showing a grain boundary in GaN.
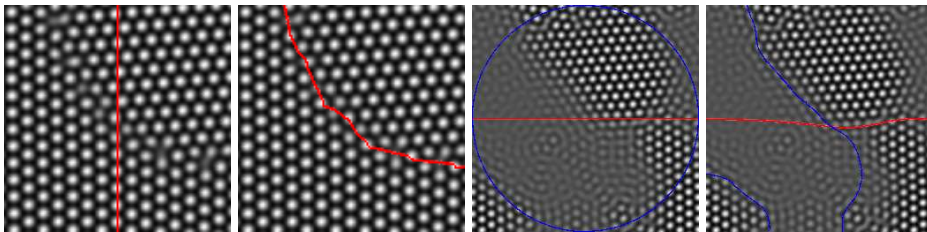

Fig. 6. Grain boundary detection on PFC simulation data: crystal phase field function u (first picture) with the initial zero level set of ψ, finally computed grain boundary (second picture). Combined grain boundary and liquid–solid interface detection on PFC simulation data: crystal phase field function u (third picture) with the initial grain boundary in red and the initial liquid–solid interface in blue, final grain boundary and liquid–solid interface location (fourth picture).

6 Conclusion

We have presented a robust method for the reliable segmentation of grain boundaries in materials science on the atomic scale. The method is based on an explicit encoding of the lattice structure and its orientation in a Mumford-Shah type variational formulation. The numerical implementation is inspired by the segmentation approach by Chan and Vese. The algorithm works equally well on phase field crystal (PFC) simulations and on experimental transmission electron microscopy (TEM) images. The method has been extended to detect also liquid–solid interfaces. At first, we confine here to two different grain orientations. The straightforward extension to 2^n orientations is currently still work in progress. On still images, the demarcation of such interfaces might be done by hand as well. But for the validation of physical models with experimental data, it is the evolution of the grain boundaries which actually matters. Here, an accurate and robust extraction of interface velocities requires a reliable automatic tool. Thus, an extension of our model to temporal data is envisaged. So far, the lattice orientation is considered as the only local degree of freedom. The type of crystal structure and the atom spacing are preset. In a future generalization one might incorporate further lattice parameters in the variational approach or combine the lattice type classification directly with the variational parameter estimation.

References

1. Antonin Aujol, Jean-François Chambolle. Dual norms and image decomposition models. *International Journal of Computer Vision*, 63(1):85–104, June 2005.
2. Jean-François Aujol, Gilles Aubert, and Laure Blanc-Feáaud. Wavelet-based level set evolution for classification of textured images. *IEEE Transactions on Image Processing*, 12(12):1634–1641, 2003.
3. Jean-François Aujol and Tony F. Chan. Combining geometrical and textured information to perform image classification. *Journal of Visual Communication and Image Representation*, 17(5):1004–1023, 2006.
4. Marc Berthod, Zoltań Kato, Shan Yu, and Josiane B. Zerubia. Bayesian image classification using markov random fields. *Image and Vision Computing*, 14(4):285–295, May 1996.
5. Charles Bouman and Michael Shapiro. Multiscale random field model for bayesian image segmentation. *IEEE Transactions on Image Processing*, 3(2):162–177, March 1994.
6. Vicent Caselles, Francine Catté, Tomeu Coll, and François Dibos. A geometric model for active contours in image processing. *Numer. Math.*, 66:1–31, 1993.
7. Tony F. Chan and Luminita A. Vese. Active contours without edges. *IEEE Transactions on Image Processing*, 10, no. 2:266 – 277, 2001.
8. Daniel Cremers and Christoph Schnörr. Statistical shape knowledge in variational motion segmentation. *Image and Vision Computing*, 21(1):77–86, January 2003.
9. G. Doretto, D. Cremers, P. Favaro, and S. Soatto. Dynamic texture segmentation. In B. Triggs and A. Zisserman, editors, *IEEE International Conference on Computer Vision (ICCV)*, volume 2, pages 1236–1242, Nice, Oct. 2003.

10. K.R. Elder and M. Grant. Modeling elastic and plastic deformations in nonequilibrium processing using phase field crystals. *Physical Review E - Statistical, Nonlinear, and Soft Matter Physics*, 70(5 1):051605–1–051605–18, November 2004.
11. Matthias Heiler and Christoph Schnörr. Natural image statistics for natural image segmentation. 63(1):5–19, 2005.
12. Wayne E. King, Geoffrey H. Campbell, Stephen M. Foiles, Dov Cohen, and Kenneth M. Hanson. Quantitative HREM observation of the $\Sigma 11(113)/[\bar{1}00]$ grain-boundary structure in aluminium and comparison with atomistic simulation. *Journal of Microscopy*, 190(1-2):131–143, 1998.
13. P. Kosmol. *Optimierung und Approximation.* de Gruyter Lehrbuch, 1991.
14. Sridhar Lakshmanan and Haluk Derin. Simultaneous parameter estimation and segmentation of gibbs random fields using simulated annealing. *IEEE Transactions on Pattern Analysis and Machine Intelligence*, 11(8):799–813, 1989.
15. B. S. Manjunath and Rama Chellappa. Unsupervised texture segmentation using markov random field models. *IEEE Trans. Pattern Anal. Mach. Intell.*, 13(5):478–482, 1991.
16. Yves Meyer. *Oscillating Patterns in Image Processing and Nonlinear Evolution Equations: The Fifteenth Dean Jacqueline B. Lewis Memorial Lectures.* American Mathematical Society, Boston, MA, USA, 2001.
17. D. Mumford and J. Shah. Optimal approximation by piecewise smooth functions and associated variational problems. *Comm. Pure Appl. Math.*, 42:577–685, 1989.
18. S. J. Osher and R. P. Fedkiw. *Level Set Methods and Dynamic Implicit Surfaces.* Springer-Verlag, 2002.
19. Nikos K. Paragios and Rachid Deriche. Geodesic active regions and level set methods for motion estimation and tracking. *Computer Vision and Image Understanding*, 97(3):259–282, March 2005.
20. Andreas Rätz and Axel Voigt. An unconditionally stable finite element discretization of the phase-field-crystal model. in preparation 2006.
21. Berta Sandberg, Tony Chan, and Luminita Vese. A level-set and gabor-based active contour algorithm for segmenting textured images. Technical Report 02-39, UCLA CAM Reports, 2002.
22. J.A. Sethian. *Level Set Methods and Fast Marching Methods.* Cambridge University Press, 1999.
23. Y. Singh. Density-functional theory of freezing and properties of the ordered phase. *Physics Reports*, 207(6):351–444, 1991.
24. Michael Unser. Texture classification and segmentation using wavelet frames. *IEEE Transactions on Image Processing*, 4(11):1549–1560, November 1995.
25. Luminita Vese and Tony F. Chan. A multiphase level set framework for image segmentation using the mumford and shah model. *International Journal of Computer Vision*, 50(3):271–293, December 2002.
26. Luminita Vese and Stanley Osher. Modeling textures with total variation minimization and oscillating patterns in image processing. *Journal of Scientific Computing*, 19(1-3):553–572, December 2003.